

STEADY FLOW AND HEAT TRANSFER AROUND AN INCLINED SQUARE CYLINDER CONFINED IN A TWO-DIMENSIONAL CHANNEL

Jaber Aboueian-Jahromi, Alireza Hossein Nezhad †, and Amin Behzadmehr ††

MS student, University of Sistan and Baluchestan, Department of Mech. Eng.,

Zahedan, Iran

E-mail: Aboueian@gmail.com

† Assistant prof., University of Sistan and Baluchestan, Department of Mech. Eng.,

Zahedan, Iran

E-mail: Nezhadd@hamoon.usb.ac.ir

†† Associate prof., University of Sistan and Baluchestan, Department of Mech. Eng.,

Zahedan, Iran

E-mail: Behzadmehr@hamoon.usb.ac.ir

Key words: Steady flow, Inclined square cylinder, Blockage ratio, Laminar channel flow, Drag coefficient, Nusselt number

Abstract. *In this study, the numerical investigation of flow and heat transfer around a heated long inclined square cylinder in a steady laminar regime is carried out for the range of conditions as $1 \leq Re \leq 40$ and $0.7 \leq Pr \leq 100$. The square cylinder is placed on the axis of a plane channel and an angle of inclination equal to 45° with a fixed blockage ratio of $1/8$ is considered. The variation of local Nusselt number on each surface of the heated square obstacle for the constant wall temperature and uniform heat flux boundary conditions are presented to elucidate the role of Prandtl number on heat transfer. The average Nusselt number increases with a growth in the Reynolds and/or the Prandtl number. This value is higher for uniform heat flux condition in comparison with constant temperature one. Simple correlations have been also obtained for the Nusselt number according to the different Reynolds and Prandtl numbers for both boundary conditions. In addition, In order to investigate the flow characteristics, results are presented in terms of streamline and vorticity contours. Under a provided correlation, the length of recirculation increases linearly with the Reynolds number.*

1 INTRODUCTION

For a long time, the study of flow around cylindrical bluff bodies of circular and square cross-sections has been subject of intense experimental and numerical researches because of the importance of these flows in numerous industrial applications such as cooling towers, gas and oil pipelines, flow-meters, chimneys, antennas, support structures, etc. Besides, the flow over a block is academically attractive, for it can be a good opportunity to study such these flow phenomena and predict characteristics of similar flows occurring in technology. Consequently, there are many works in the literature relating to different aspects of flows around cylinders surveying characteristics of hydrodynamics and heat transfer.

However, in the case of a square cross-section cylinder, the separation points are fixed because the square cylinder has four sharp edges with flat wall surfaces. Recently, Dhiman et al. [1] reviewed different flow regimes according to the different values of the Reynolds numbers among the considerable amount of data gathered for square cylinder with one side facing the flow: there is a creeping flow with no flow separation at the surface of the cylinder for $Re \leq 1$. Then by increasing the Reynolds number a closed steady recirculation region is observed behind the bluff body. This recirculation region enlarges with increasing Re and at a critical Reynolds number ($50 < Re < 70$), a von Karman vortex street forms in the flow field the flow becomes unsteady. When the Reynolds number is further increased ($100 \leq Re \leq 200$), the separation points go to the leading edges of the cylinder and after around $Re = 160$, a three-dimensional flow in an unbounded geometry is detected. The onset of this three-dimensional flow is not fully investigated yet in the literature. In that work, Dhiman et al. [1] studied the effects of Reynolds ($1 \leq Re \leq 45$) and Prandtl ($0.7 \leq Pr \leq 4000$) numbers on the characteristics of cross flow and heat transfer of Newtonian fluids around a confined square cylinder.

Davis et al. [2] presented both numerical and experimental results for confined flow around rectangular cylinders for two blockage ratios ($\beta = 1/4$ and $1/6$) and three rectangular aspect ratios ($A = 0.6, 1$ and 1.7) at Reynolds numbers ranging from 100 to 1850. They found that the presence of confining walls and the form of upstream velocity profile lead to numerous changes in the characteristics of the flow around rectangles.

Breuer et al. [3] conducted a two dimensional study for a confined flow around a square cylinder mounted inside a plane channel with a blockage ratio of $1/8$ by two different numerical techniques, namely a Lattice Boltzmann Equation (LBE) and a finite volume method (FVM) in the Reynolds number range $0.5 \leq Re \leq 300$ with a parabolic velocity profile at the channel inlet. They evaluated the integral quantities such as drag coefficient, recirculation length and Strouhal number for both steady ($0.5 \leq Re \leq 60$) and unsteady ($60 \leq Re \leq 300$) flows and found an excellent agreement between LBE and FVM.

Turki et al. [4] have numerically studied the forced and mixed convection around a heated square cylinder mounted inside a horizontal channel for the two-dimensional unsteady flow region $62 \leq Re \leq 200$ at Richardson numbers (Ri) up to 0.1 for two blockage ratios of $1/4$ and $1/8$. In pure forced convection the value of the critical Reynolds number (onset of periodic flow) increases with increasing the blockage ratio. In mixed convection, the critical value of Reynolds number decreases with increasing the Richardson number. They also proposed the Nusselt number correlations for forced and mixed convections.

Gupta et al. [5] studied the heat transfer of power-law liquids around a confined square cylinder for $5 \leq Re \leq 40$, $0.5 \leq n \leq 1.4$ and $1 \leq Pr \leq 10$ ($5 \leq Pe \leq 400$) for both constant wall temperature (CWT) and uniform heat flux (UHF) conditions on the surface of cylinder for a fixed blockage ratio of $1/8$ on uniform staggered grid arrangement in a long channel with a parabolic velocity profile at the channel inlet and Orlanski condition at the channel outlet.

Relatively shorter wake regions in shear-thinning liquids than shear-thickening liquids are observed. The effect of the Reynolds number on the flow patterns is qualitatively similar to that seen for Newtonian fluids. On the whole, heat transfer is fascinated for shear-thinning behaviors of liquids and hampered for shear-thickening behaviors.

While the flow over the square cylinder obey the regime with the fixed separation points at the leading edges, the aerodynamics are relatively insensitive to the Reynolds number, but are more sensitive to the angle of incidence [6]. Consequently it is quite likely that the flow characteristics, aerodynamic forces, vortex shedding frequency, heat-transfer performance, etc., will exhibit distinct behaviors in different ranges of incidence angle of the square cylinder [7].

Sohankar et al. [8] studied the onset of vortex shedding and the influence of outlet boundary conditions and blockage ratio for unsteady Newtonian flow over a square cylinder at incidence ($0 \leq \alpha \leq 45^\circ$) confined in a 2D channel and exposed to a constant free stream velocity for the range of $45 \leq Re \leq 200$ (Re based on constant entrance velocity and projected diameter of square). They concluded that when a square cylinder is inclined with respect to the direction of the main flow, flow separation may occur at various pairs of the edges of the square, resulting in drastic change of the key flow parameters such as force coefficients and the Strouhal number. Conjecturing that the critical Reynolds number increases with increasing blockage ratio, they obtained the critical Reynolds based on diameter of cylinder for onset of vortex shedding at a blockage of 5% and an incidence angle of $\alpha = 45^\circ$ equal to 42.

Yoon et al. [9] numerically investigated feasibility of using large-scale vortices to enhance heat transfer on a channel wall with constant heat flux by using an adiabatic square cylinder at different incidence angles θ at $Re = 500$ and 750 . Obtaining the maximum enhancement at $\theta = 45^\circ$, they found that vertical velocity fluctuation plays a key role in convective heat transfer on the channel wall and so an inclined square cylinder is an effective tool to control heat transfer in channel flows.

Moussaoui et al. [10] simulated two-dimensional incompressible flow and heat transfer in a horizontal channel differentially heated and obstructed by an inclined square cylinder with an angle of 45° to the flow for the Reynolds numbers ranging $0 \leq Re \leq 300$, $Pr = 0.7$ and the blockage ratio of $\beta = 1/4$, using a strategy based on lattice Boltzmann for fluid velocity fields and finite difference for temperature. They imposed a fully developed profile at the inlet and the Neumann boundary condition, i.e., setting the stream wise gradients of the velocity and temperature to zero, at the outlet. They found that the critical Reynolds number (based on the square diameter and the maximum inlet velocity) for onset of vortex shedding is about 82.

Most of the scant available literatures on the fluid flow over an inclined square cylinder are in unsteady region surveying the vortex shedding phenomenon. On the other hand much less attention has been devoted to heat transfer characteristics. The studies on the effects of the Prandtl number on heat transfer haven't been of interest to scientists over the years. However it is readily admitted that in chemical, petroleum and oil related industrial applications the values of Prandtl number up to 100 are frequently encountered.

Recently, little prior work is carried out on the effect of Prandtl number on the forced and mixed convection heat transfer from cylinders of circular or square (with no angle of attack) cross section, but there is no numerical results in the literature on the effects of Prandtl number on the heat transfer coefficients around an inclined square cylinder. Therefore, the main purpose of the present work is to study and correlate the heat transfer characteristics for an inclined square cylinder with emphasis on the effects of the different Prandtl numbers in a wide range ($0.7 \leq Pr \leq 100$) for a fixed blockage ratio of $\beta = 1/8$.

2 PROBLEM STATEMENT AND GOVERNING EQUATIONS

The system of interest here is the steady, incompressible, two dimensional laminar flow of Newtonian fluids past a square cylinder (diameter = b) at an incidence angle of 45° with respect to the channel centerline and symmetrically confined inside an adiabatic channel (Fig. 1). Two different thermal boundary conditions on the square cylinder surfaces are considered here: constant wall temperature (CWT) and uniform heat flux (UHF). The aim is to simulate an infinitely long channel. However, as the computational domain has to be finite, a fully developed parabolic velocity profile, with the maximum value of U_{max} , and a constant temperature of T_{in} is enforced at the inlet of the channel, while, the Neumann boundary condition (NBC) is imposed at the outlet. The thermo-physical properties of streaming liquid are assumed to be independent of temperature; furthermore, the viscous dissipation effects are also assumed to be negligible. These two assumptions restrict the applicability of the results to the situations where the maximum temperature difference and the Brinkman number in the flow domain remain low enough in order to satisfy the temperature independency and viscous dissipation negligibility, respectively. The Brinkman number provides an adequate estimate of the ratio between the heat generated by viscous heating and the heat exchanged at the wall [11]. The distance from the inlet plane to the front corner of the obstacle (upstream distance) is X_u , and the distance between the rear corner and the exit plane (downstream distance) is X_d . The total non-dimensional length of the computational domain is L_2/b in the axial direction. The non-dimensional height in the lateral direction, L_1/b , defines the blockage ratio ($\beta = b/L_1$). A constant blockage ratio of $\beta = 1/8$ has been used in this work.

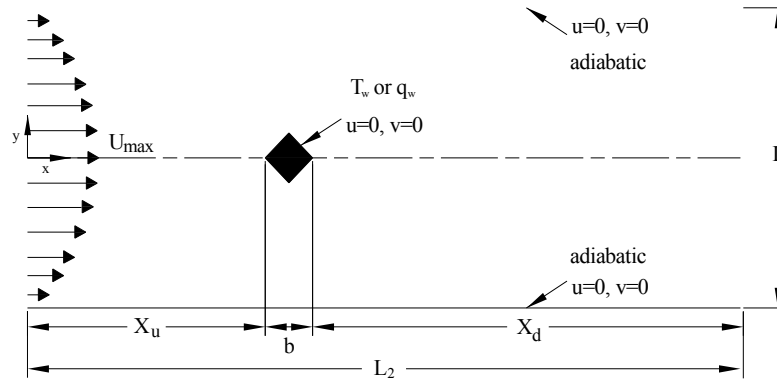


Figure 1: Schematic of a confined flow over an inclined square cylinder

The governing equations in their dimensionless forms, i.e., the continuity, the x- and y-components (assuming negligible buoyancy effects) of the Navier-Stokes and the thermal energy equations (assuming negligible viscous dissipation and constant thermo-physical properties) are written as follows:

Continuity:

$$\frac{\partial u^*}{\partial x^*} + \frac{\partial v^*}{\partial y^*} = 0 \quad (1)$$

x-Momentum:

$$u^* \frac{\partial u^*}{\partial x^*} + v^* \frac{\partial u^*}{\partial y^*} = -\frac{\partial p^*}{\partial x^*} + \frac{1}{Re} \left[\frac{\partial^2 u^*}{\partial x^{*2}} + \frac{\partial^2 u^*}{\partial y^{*2}} \right] \quad (2)$$

y-Momentum:

$$u^* \frac{\partial v^*}{\partial x^*} + v^* \frac{\partial v^*}{\partial y^*} = -\frac{\partial p^*}{\partial x^*} + \frac{1}{Re} \left[\frac{\partial^2 v^*}{\partial x^{*2}} + \frac{\partial^2 v^*}{\partial y^{*2}} \right] \quad (3)$$

Energy equation:

$$u^* \frac{\partial T^*}{\partial x^*} + v^* \frac{\partial T^*}{\partial y^*} = \frac{1}{Pe} \left(\frac{\partial^2 T^*}{\partial x^{*2}} + \frac{\partial^2 T^*}{\partial y^{*2}} \right) \quad (4)$$

The boundary conditions for the momentum and energy equations in their dimensionless forms may be written as (Fig. 1):

Inlet boundary:

$$u^* = 1 - |2\beta y^*|^2, v^* = 0, T^* = 0$$

where $\beta = b/L_1$ and $-L/2b \leq y^* \leq L/2b$.

Upper and lower boundary:

$$u^* = 0, v^* = 0, \frac{\partial T^*}{\partial y^*} = 0$$

Square cylinder:

$$u^* = 0, v^* = 0, T^* = 1 (CWT) \text{ or } \frac{\partial T^*}{\partial n_s^*} = -1 (UHF)$$

Where n_s^* is the dimensionless normal direction of cylinder surface.

Outlet boundary:

$$\frac{\partial u^*}{\partial x^*} = 0, \frac{\partial v^*}{\partial x^*} = 0, \frac{\partial T^*}{\partial x^*} = 0$$

Without assuming the symmetry of the flow about the centerline of the channel, numerical solution of governing equations in conjugation with the above-mentioned boundary conditions are solved to obtain the velocity $u^*(x^*, y^*)$, $v^*(x^*, y^*)$, pressure $p^*(x^*, y^*)$ and temperature $T^*(x^*, y^*)$ fields in the full domain (Fig. 1). The fully converged velocity field has been used as an input to solve thermal energy equation. These fields, in turn, are used to deduce the values of integral quantities and of the derived variables like stream function and vorticity. In this study, the local Nusselt number is defined as $Nu_{local} = -\partial T^* / \partial n_s^*$ and $Nu_{local} = 1/T_w^*$ for the constant temperature and constant heat flux boundary conditions, respectively. So for a fixed geometry, there are two effective (Re and Pr) and two effected (C_D and Nu) dimensionless parameters in this problem.

3 NUMERICAL SOLUTION PROCEDURES

3.1 Grid Structure

The grid structure used in the present work is shown in figure 2. It shows grid structure for the whole computational domain. It consists of separate zones with uniform and non-uniform grid distribution having fine grids in the regions of large gradients and coarser grids in the regions of low gradients. There are three different grid distributions in the centerline of the channel in x-direction. There are the finest uniform grids with a constant cell size, δ , in an inner region around the obstacle over a distance of $1.5b$ to capture wake-wall interactions in

both directions. The coarsest uniform grid distribution in x-direction with a constant cell size, $\Delta = 0.25b$, is applied in an outer region that extends beyond $8.5b$ from the inlet surface and $16.5b$ from the outlet surface of the channel toward the obstacle. A scheme with constant ratio of any two succeeding interval lengths has been used for stretching the cell sizes between these limits of δ and Δ in the x-direction. A similar scheme is employed symmetrically for generating the grid points extending from $0.25b$ of the side corners of the body to the channel walls in the y-direction. A fine grid size, δ , is also clustered near the upper and lower walls of the channel. A scheme using quadrilateral grid elements is also used in x-y direction to mesh the triangular gaps around the uniform grids beside the cylinder (figure 2(b)).

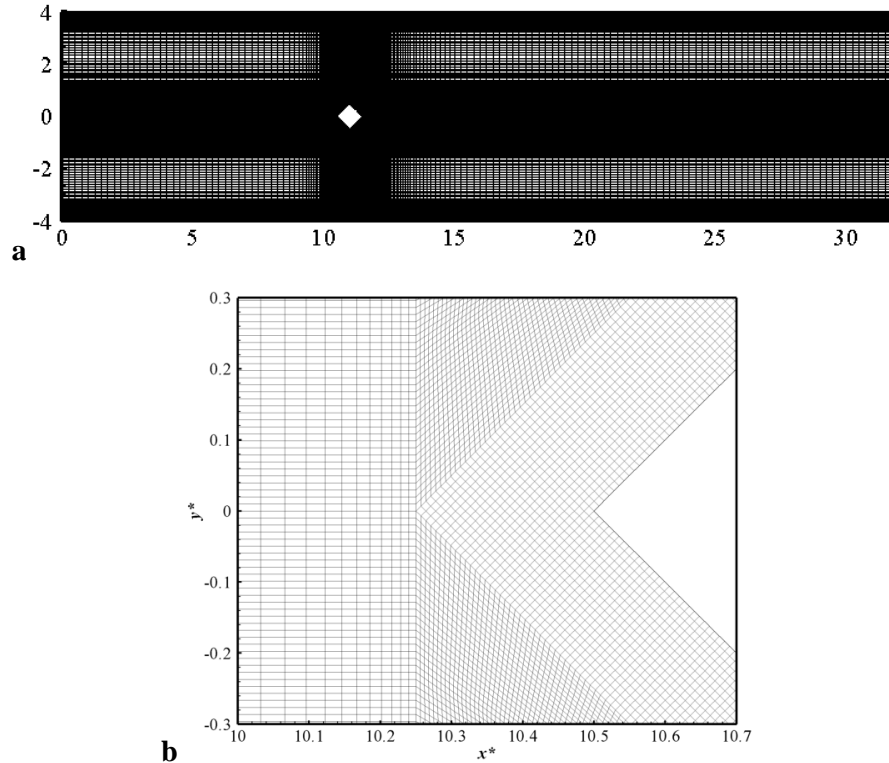


Figure 2. Non-uniform computational grid structure with 330×315 ($x \times y$) grid points: (a) computational domain (b) close up the cylinder

3.2 Numerical Details

The governing equations subjected to the aforementioned boundary conditions are solved using a finite volume based code according to the semi-implicit method for the pressure linked equations (SIMPLE) algorithm. A second-order upwind scheme is used to discretize the convective terms in the momentum and thermal energy equations, while the diffusive terms are discretized using central differences. The velocity fields obtained by solving the Navier Stokes equations are used as an input to the thermal energy equation. Convergence criteria of 10^{-10} for the continuity and x - and y -components of the velocity and 10^{-15} for the temperature were prescribed in this work.

3.3 Domain and Grid Independence

The accuracy and reliability of the numerical results is contingent upon the choice of an optimal grid and upstream and downstream distances describing the flow domain. In this

research, the non-dimensional upstream and downstream distances of the computational domain are selected $X_u/b=10.5$ and $X_d/b=20.5$, respectively (figure 1). These values are chosen based on the performed studies in the present work to reduce the effects of inlet and outlet boundary conditions on the flow and heat transfer characteristics near the obstacle. In order to explore the influence of the assumed finite domain, additional computations have been carried out for the two extreme values of the Reynolds number ($Re=1$ and 40), each for the two extreme values of Prandtl number ($Pr=1$ and 100) for both thermal boundary conditions in study of domain and grid independence. However, just the maximum values of changes are mentioned here.

Therefore, in order to find the appropriate value of upstream distance, It can be announced that increasing the upstream extent from 8.5 and 10.5 to 13.5 (having downstream distance constant ($X_d/b=20.5$)) produces the maximum percentage change of 0.07% and 0.02% in the value of the drag coefficient (C_D) for $Re=40$, respectively, while the upmost percentage changes in the values of the average Nusselt numbers for $X_u/b=8.5$ and 10.5 are 0.18% and 0.05% with respect to the value of average Nusselt number for $X_u/b=13.5$ at $Re=1$, $Pr=1$ for both thermal boundary conditions.

Furthermore, while the downstream distance is increased, for the constant value of upstream ($X_u/b=10.5$), the maximum changes in the value of C_D and Nu occur at $Re=40$ and $Pr=1$. The relative percentage changes for these Re and Pr numbers in the values of C_D are 0.88%, 0.24% and 0.006% for $X_d/b=4.5$, 6.5 and 10.5 as compared to $X_d/b=20.5$, respectively. The same comparison for the values of the average Nu leads to the percentage changes of 0.16%, 0.04% and 0.001%, respectively. In addition, it is found that an increase from $X_d=20.5$ to 30 gives negligible influences on global flow and heat transfer quantities (less than 0.01%).

Table 1: Grid independence study of C_D and Nu for $Re=40$ (CWT)

Grid	δ	Grid size ($M \times N$)	No. of cells	C_D	Nu ($Pr=1$)	Nu ($Pr=100$)
G1	0.03	136 × 205	28404	1.5906	3.7252	20.8033
G2	0.02	186 × 241	45538	1.5962	3.7159	19.9335
G3	0.01	186 × 241	50310	1.6028	3.7074	19.2426
G4	0.01	250 × 335	87826	1.6028	3.7077	19.2140
G5	0.01	314 × 329	107390	1.6032	3.7085	19.2216
G6	0.008	292 × 380	117504	1.6042	3.7068	19.1280

M Number of cells on the channel entrance line, N number of cells on the channel walls, δ grid spacing in the $1.5b$ region around the cylinder

Having fixed the domain size, the grid independence has been carried out by using different non-uniform structured grids for the same values of Reynolds and Prandtl numbers. In grid study, it was seen that the maximum percentage changes in the values of the drag coefficient and the average Nusselt number mostly occurred for maximum values of Re and Pr numbers ($Re=40$ and $Pr=100$) for both thermal boundary conditions on the cylinder surface (CWT and UHF). Table 1 shows the effects of six different grid structures on the drag coefficient and the average Nusselt number for $Re=40$ and the maximum and minimum values of Prandtl number ($Pr=1$ and 100) for constant wall temperature boundary condition. The refinement in the grid from G5 to G6 shows 0.06%, 0.05% and 0.49% changes for C_D , Nu (for $Pr=1$) and Nu (for $Pr=100$), respectively. Therefore the grid G5 (314! 329 and $\delta=0.01$) is believed to be sufficiently refined to simulate flow and heat transfer phenomena.

4 RESULTS AND DISCUSSION

In order to examine the influence of the inclined square obstacle upon the flow and temperature field inside the channel, steady flow numerical computations have been carried out using the full domain ($-L/2b \leq y^* \leq L/2b$) for the following values of dimensionless parameters: Reynolds number, $Re=1, 5, 10, 20, 30$ and 40 ; Prandtl number, $Pr=1, 5, 10, 20, 50$ and 100 and for the constant value of blockage ratio, $\beta = 1/8$. The role of two classical thermal boundary conditions, i.e., CWT and UHF has also been examined for the above range of conditions.

4.1 Validation of Results

In order to judge the accuracy of the obtained results for the inclined square cylinder at incidence angle, $\alpha = 45^\circ$, the fluid flow and the heat transfer around a square cylinder with no angle of incidence ($\alpha = 0^\circ$) are also studied and their results are compared with the existing results [1 and 3]. In figure 3(a), total drag coefficient is presented and compared with the results given by Dhiman et al. [1] and Breuer et al. [3] for a confined flow around a cylinder with square cross-section mounted inside a plane channel with a blockage ratio of $1/8$ for $Re = 10, 20, 30$ and 40 (both using finite volume method with 100 control volumes on each face of the cylinder). Furthermore, for accrediting the obtained heat transfer characteristics, a comparison of the present values of the average Nusselt number on the cylinder with those of Dhiman et al. [1] is presented in Table 2. On the other hand, for validating the results within the desired inclination angle, a comparison on the total drag coefficient is done in figure 3(b) with the results of Moussaoui et al. [10] for an inclined square cylinder ($\alpha = 45^\circ$) confined in a channel with a blockage ratio of $1/4$ for $Re = 20, 30, 40, 50$ and 60 . As can be seen, our results compare favorably graphically with those reported by others in these figures. A small deviation between the numerical results depends on the different grids used, solution algorithm, numerical errors due to iteration, round-up and programming and so on. For example, the maximum deviations between the obtained drag coefficients and the results of Dhiman et al. [1] and Breuer et al. [3] in figures 3(a) are about 2% and 4.5%, respectively.

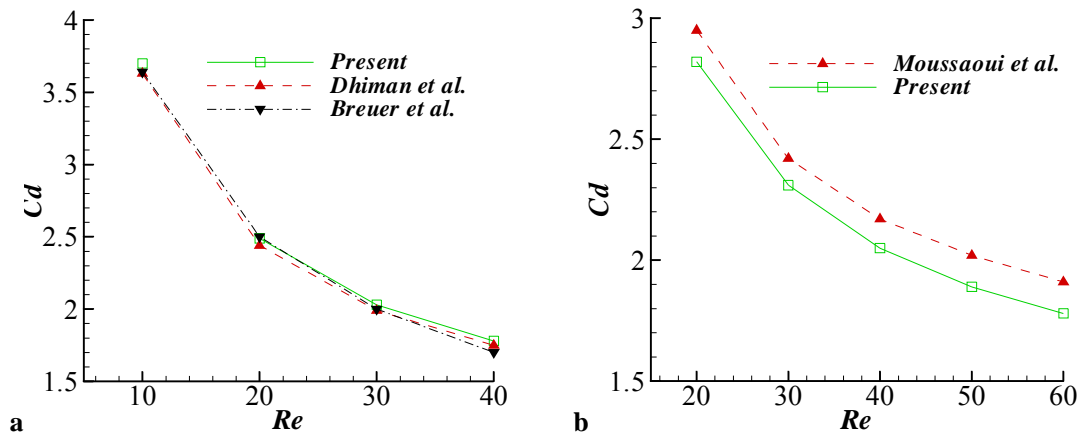


Figure 3: comparison with previous works (a) straight square for $\beta = 1/8$, (b) inclined square for $\beta = 1/4$

These deviations are about 7.3% and 1.6% in figure 3(b) and table 2 respectively for C_D and Nu . The non-dimensional wake lengths are also exactly similar to the values reported by Dhiman et al. [1] for all Reynolds numbers studied here.

Table 2. Comparison of Nu with the literature values ($\alpha = 0, \beta = 1/8$)

Pr	$Re = 10$		$Re = 20$		$Re = 30$		$Re = 40$	
	10	100	10	100	10	100	10	100
Present	3.67	7.58	4.82	10.37	5.75	12.53	6.53	14.28
Dhiman et al. [1]	3.66	7.64	4.88	10.41	5.69	12.52	6.59	14.15

4.2 Flow Patterns

Figure 4 elucidates representative streamline and vorticity profiles around the inclined square cylinder for different Reynolds numbers ranging from 1 to 40. It is clearly seen in figure 4(a) and (b) (for $Re = 1$ and 5, respectively) that a creeping steady flow with no separation points pasts the inclined square cylinder as viscous forces dominate the flow. As the Reynolds number increases, the flow separation occurs at a Reynolds number between 5 and 10 and two small symmetric vortices, rotating in opposite directions, are observed in the recently created wake region behind the obstacle. The size of these vortices grows with an increase in the Reynolds number (figure 4(c)-(f)). The vorticity profiles can also be used to locate the separation points and to investigate the behavior of the fluid flow, especially near the solid walls. The maximum magnitude of the vorticity is seen to occur around the side edges of the obstacle. The vorticity profiles are also moved towards the flow with rising Reynolds number.

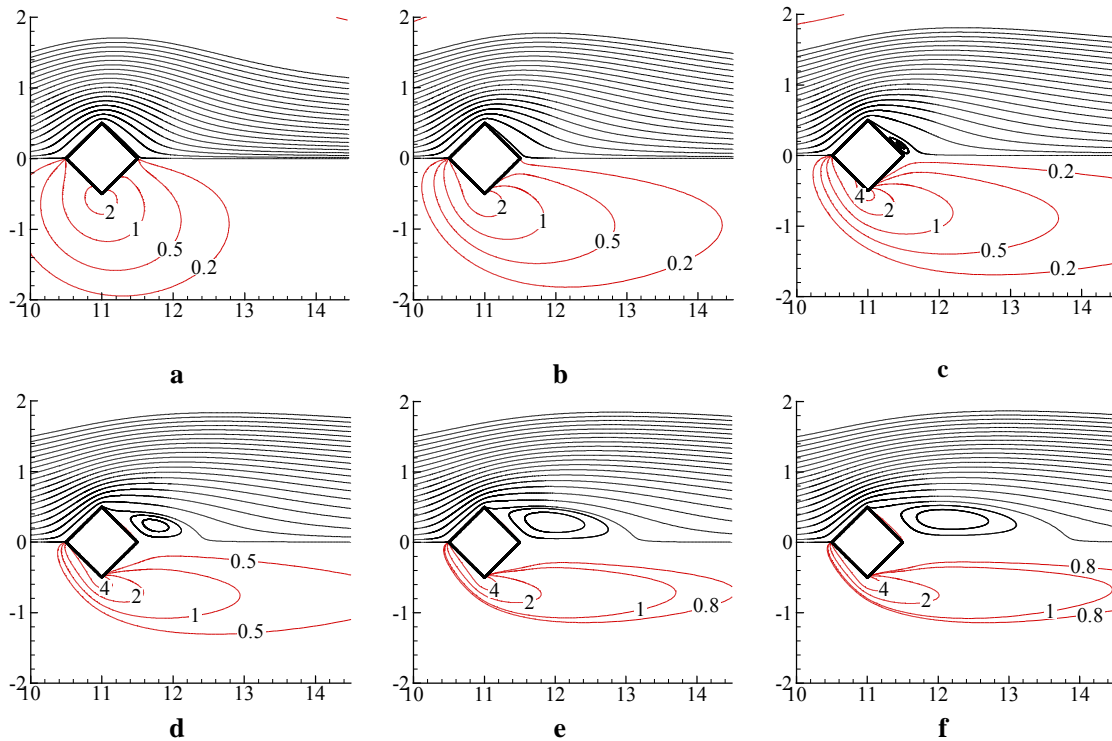


Figure 4: Streamline and vorticity profiles (upper and lower half present the results for streamline and vorticity, respectively) for (a) $Re = 1$, (b) $Re = 5$, (c) $Re = 10$, (d) $Re = 20$, (e) $Re = 30$ and (f) $Re = 40$ at $\beta = 1/8$

4.3 Recirculation Length

Figure 5(a) shows the computed results for the non-dimensional recirculation length L_r (defined as the distance from the rare edge of the obstacle to the point of attachment for the near closed streamline on the axis of symmetry at $y = 0$) as a function of the Reynolds number. The length of the recirculation region is seen to increase linearly with Reynolds number. Zdravkovich [12] suggested the linear empirical relation the recirculation length for an unconfined circular cylinder as:

$$L_r / b = 0.05Re \quad \text{for } 4.4 \leq Re \leq 40. \quad (5)$$

Dhiman et al. [1] also proposed the following linear relationship between the recirculation length and Reynolds number for a straight square cylinder with a blockage ratio of 1/8 in the steady flow regime:

$$L_r / b = -0.0732 + 0.0563Re \quad \text{for } 5 \leq Re \leq 45. \quad (6)$$

Similarly to the relationship (6) for the straight square cylinder, a curve fit of the present inclined square cylinder results ($\beta = 1/8$) leads to

$$L_r / b = -0.618 + 0.072Re \quad \text{for } 10 \leq Re \leq 40. \quad (7)$$

According to this derived equation, the onset of separation can be predicted at $Re \approx 8.6$. It can be announced that the recirculation length of the inclined square cylinder flow in comparison with the straight square cylinder (for similar blockage ratio of 1/8) and the circular cylinder flows (in free stream) is slightly shorter for Reynolds number below $Re \approx 34.7$ and 11.6, respectively and larger above these values.

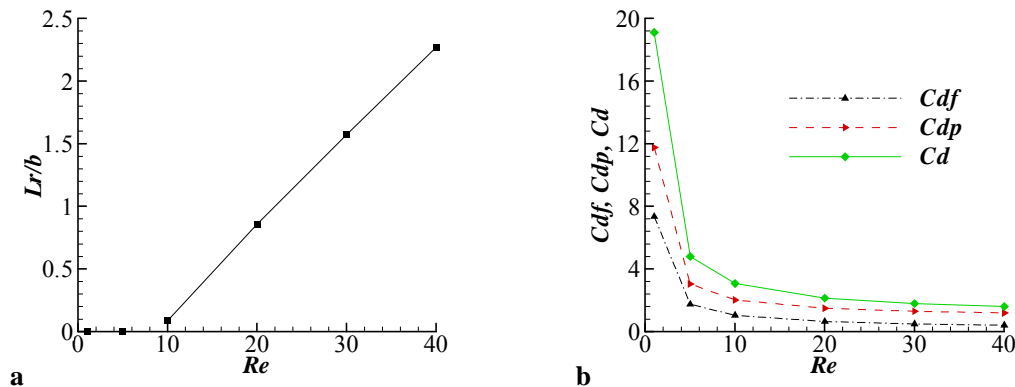


Figure 5: Variation of recirculation length (a) and drag coefficients (b) versus Reynolds number

4.4 Drag Coefficients

One of the most important parameters for flow around an obstacle is the drag coefficient C_d . The drag exerted on the obstacle is made up of two components: viscous drag and pressure drag. Non-dimensional form of each of these components is defined as viscous drag coefficient ($C_{df} = F_{df} / (1/2 \rho U_{max}^2 b)$) and pressure drag coefficient ($C_{dp} = F_{dp} / (1/2 \rho U_{max}^2 b)$) and therefore the total drag coefficient is $C_d = C_{df} + C_{dp}$. Figure 5(b) depicts the variation of these components against Reynolds number. As expected, in the steady state flow region, due to diminishing effect of viscous force, the values of the individual and total drag coefficients decrease with an increase in Re . These reductions of drag coefficients are greater at low Reynolds numbers.

4.5 Local Nusselt Number

Owing to the underlying inherent differences, the results for the two boundary conditions are discussed separately.

4.5.1 Constant Wall Temperature (CWT) Condition

The variation of the local Nusselt number on the top surfaces of the cylinder (the down surfaces are symmetric) at $Re = 1, 10, 20$ and 40 for various values of Prandtl numbers is shown in figure 6. As expected, the Nusselt number increase with an increase in the Reynolds and/or Prandtl number. These plots show a sharp increase in the values of Nusselt numbers at each corner of the cylinder due to the large temperature gradient normal to the surface of the obstacle. On each surface of the cylinder, there exist a minimum as the Nusselt number increases again at the next edge. With increasing the value of the Reynolds number, this minimum goes near the top edge on the rear surface because of the changes that occurs in the mechanisms of heat transfer by the stronger vortices.

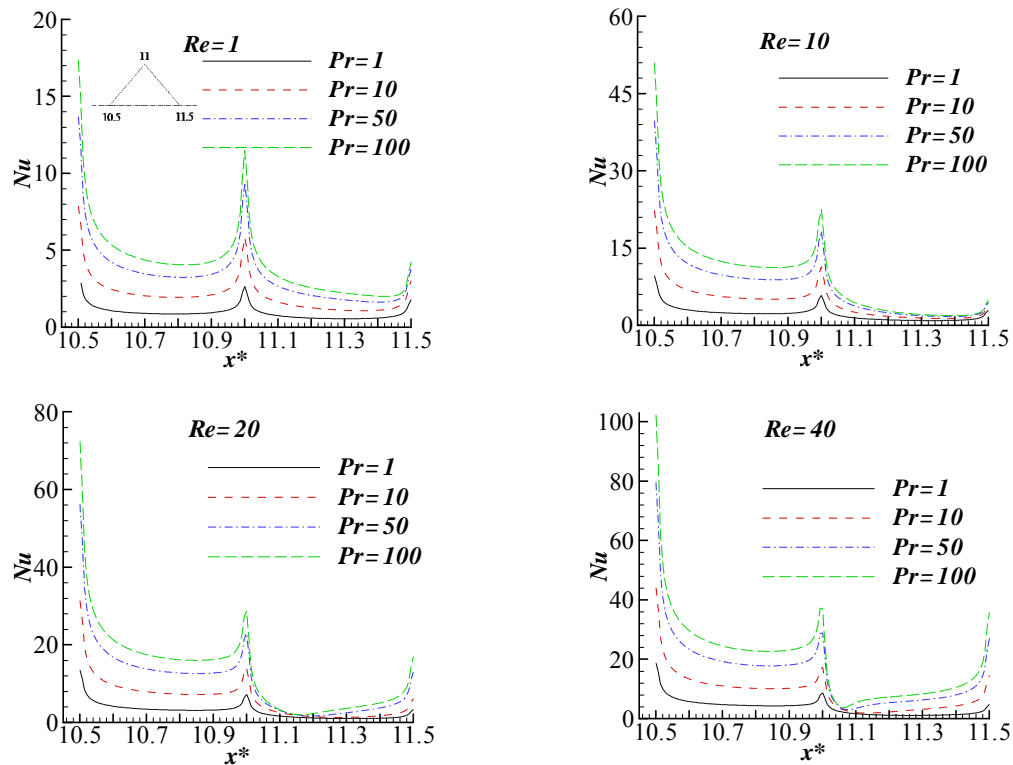


Figure 6: Local Nusselt number variation along the cylinder top surfaces (specified by its non-dimensional x -distance) for $Re = 1, 10, 20$ and 40 and $Pr = 1, 10, 50$ and 100 for CWT case.

4.5.2 Uniform Heat Flux (UHF) Condition

Representative results on the variation of local Nusselt number for top half of the inclined square cylinder along the cylinder surfaces for this case are shown in figure 7 for ranges of Reynolds and Prandtl numbers. These plots show qualitatively similar features as seen in figure 6 for the CWT condition. There are only smoother increases in the values of the Nusselt numbers at the cylinder edges.

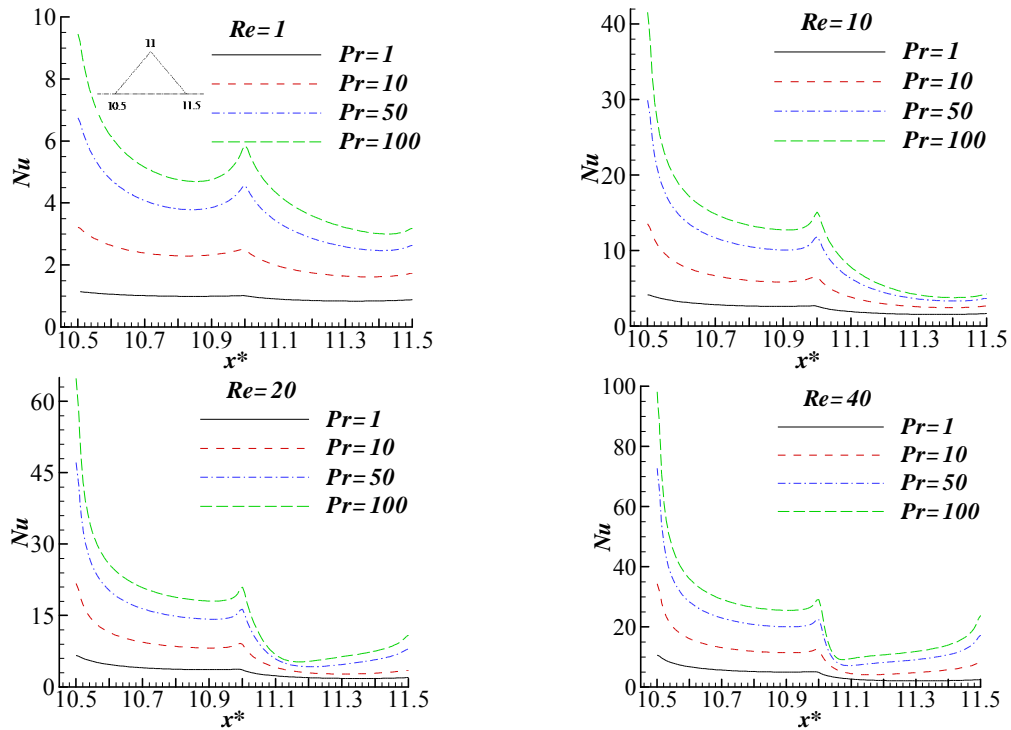


Figure 7: Local Nusselt number variation along the cylinder top surfaces (specified by its non-dimensional x-distance) for $Re = 1, 10, 20$ and 40 and $Pr = 1, 10, 50$ and 100 for UHF case.

4.6 Average Nusselt Number

The average Nusselt number for front surface (Nu_f) and rear surface (Nu_r) of the square cylinder is obtained by averaging the local Nusselt number over the each face of the obstacle. Finally, as the heat transfer area is the same for each surface the square obstacle, the overall average Nusselt number is simply the mean of the surface average values of the Nusselt number corresponding to the four surface of the cylinder. The average Nusselt number can be used in process engineering design calculations to estimate the rate of heat transfer from the cylinder in the CWT case, or to estimate the averaged surface temperature of the cylinder for the UHF condition.

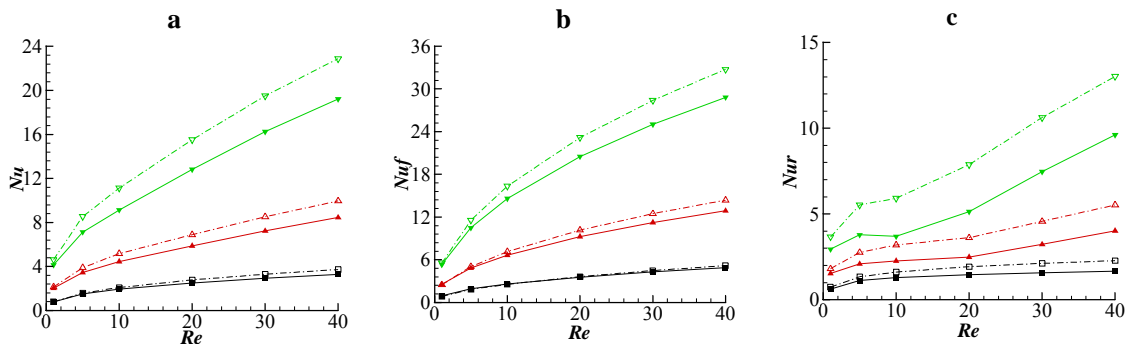


Figure 8: Average Nusselt number of the cylinder(a) and its front (b) and rear (c) faces versus Reynolds for different Prandtl numbers: (■) $Pr = 0.7$, (▲) $Pr = 50$ and (▼) $Pr = 100$ for constant temperature (filled symbols) and uniform heat flux (open symbols).

4.6.1 Constant Temperature Case

Figures 8(a)-(c) show the variation of the average Nusselt number for the square cylinder and each of its faces with Reynolds number for various Prandtl numbers. This figure shows that the average Nusselt number for the front surface is higher than the rear one. It is also seen that the average Nusselt number for the cylinder and each of its faces increases with increasing Reynolds and/or Prandtl numbers.

Correlating the present heat transfer results by simple expressions is convenient, especially for engineering applications. Further data analysis exhibits the classical dependence of the Nusselt number on Prandtl number, i.e. $Nu \propto Pr^{1/3}$. So, the important parameter for process engineering design calculations, the Colburn j -factor, is usable here:

$$j = \frac{Nu}{(Re Pr^{1/3})} \quad (8)$$

The main use of this parameter lies in the fact that it affords the possibility of reconciling the results for a range of values of Reynolds and Prandtl numbers into a single curve. The

Colburn j -factor is represented as a function of Reynolds number at different Prandtl numbers for the constant temperature case in figure 9(a). The variation is seen to be approximately linear on a logarithmic scale. The j -factor decreases with Reynolds number. The best single non-linear curve fit for all the results presented in figure 9(a) with a range of conditions $1 \leq Re \leq 40$ and $0.7 \leq Pr \leq 100$ can be obtained as:

$$j = 0.8818 \times Re^{-0.6091} \quad (9)$$

This correlation admits the low rate of heat transfer at low Reynolds numbers and the high rate at high Reynolds numbers. This expression has average and maximum deviations of the order of 4% and 11%, respectively.

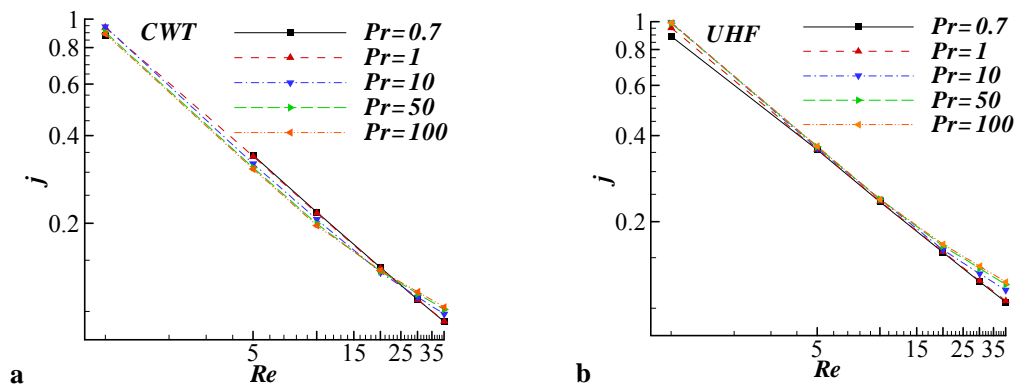


Figure 9: The Colburn j factor versus Reynolds number at various Prandtl numbers for constant wall temperature (a) and uniform heat flux (b) cases.

4.6.2 Uniform Heat Flux Case

The variation of average Nusselt number for the inclined square cylinder, and each of its faces, as a function of Reynolds number for different values of Prandtl numbers for the UHF case is shown in figures 8(a)-(c). The dependence of the average Nusselt number on the

Reynolds and Prandtl numbers seen in these figures is qualitatively similar to that observed for the condition of constant wall temperature. As expected, the mean values for the cylinder and its faces are somewhat larger than those obtained for the CWT case at the same values of Pr and Re .

Figure 9(b) also shows the functional dependency of the j -factor on the flow and heat transfer parameters for the UHF condition. These results are also seen to collapse on one curve for various Prandtl numbers in the steady flow regime. The reasonable correlation of numerical data for the range of conditions $1 \leq Re \leq 40$ and $0.7 \leq Pr \leq 100$ is given by:

$$j = 0.9399 \times Re^{-0.5816} \quad (10)$$

This shows average and maximum deviations of 4% and 12%, respectively. Attention to equations (9) and (10) also confirms the higher average Nusselt number for the UHF condition than that for CWT condition.

It should be implied that these correlations allow an easy calculation of the Nusselt number even when there is moderate variations in the values of the Prandtl numbers due to temperature dependency of thermo-physical properties. Since the average Nusselt number is related to the third root of the Prandtl number ($Nu \propto Pr^{1/3}$), even a 100% growth in the Prandtl number value will change the Nusselt number only by 26% [13]. So from an engineering application viewpoint, the assumption of the constant thermo-physical properties is not as poor as it seems.

5. CONCLUSIONS

A lack of accurate and detailed data was found in the literature for the steady flow and heat transfer around a confined inclined square cylinder which initiated the present work. In this study, the effects of Reynolds and Prandtl numbers on the flow and heat transfer characteristics of Newtonian fluids across the inclined square cylinder confined in a two-dimensional channel has been investigated for varying range of Reynolds number ($1 \leq Re \leq 40$) and Prandtl number ($0.7 \leq Pr \leq 100$) for the constant wall temperature (CWT) and uniform heat flux (UHF) conditions on the surface of cylinder. The effects of these two types of thermal boundary conditions on the Nusselt number have also been studied. Generally, the use of UHF boundary condition yields slightly higher values of the Nusselt number than those for CWT case under identical conditions of Re and Pr . The difference in the computed values of the average Nusselt number for the two types of thermal boundary conditions increases as the Reynolds or Prandtl number is increased. It is so worthwhile to have some idea about the detailed flow structures in order to analyze the heat transfer results. For this reason, the streamline and vorticity contours are also presented. It is observed that the flow separates from the cylinder side corners in the range of $5 \leq Re \leq 10$. The length of recirculation zone is also seen to increase almost linearly with the Reynolds number. The local Nusselt number at each corner of the inclined square cylinder and the average Nusselt number increase with an increase in the Reynolds number and/or Prandtl. Finally, simple new heat transfer correlations have been obtained for both the thermal boundary conditions.

REFERENCES

- [1] A.K. Dhiman, R.P. Chhabra, V. Eswaran, Flow and heat transfer across a confined square cylinder in the steady flow regime: effect of Peclet number, *Int. J. Heat Mass Transfer* 48 (2005) 4598–4614.

- [2] R.W. Davis, E.F. Moore, L.P. Purtell, A numerical-experimental study of confined flow around rectangular cylinders, *Phys. Fluids* 27 (1984) 46–59.
- [3] M. Breuer, J. Bernsdorf, T. Zeiser, F. Durst, Accurate computations of the laminar flow past a square cylinder based on two different methods: lattice-Boltzmann and finite-volume, *Int. J. Heat Fluid Flow* 21 (2000) 186–196.
- [4] S. Turki, H. Abbassi, S.B. Nasrallah, Two-dimensional laminar fluid flow and heat transfer in a channel with a built-in heated square cylinder, *Int. J. Thermal Sci.* 42 (2003) 1105–1113.
- [5] A.K. Gupta, A. Sharma, R.P. Chhabra, V. Eswaran, Two-dimensional steady flow of a power law fluid past a square cylinder in a plane channel: momentum and heat transfer characteristics, *Ind. Eng. Chem. Res.* 42 (2003) 5674–5686.
- [6] Okajima, A., Strouhal numbers of rectangular cylinders, *Journal of Fluid Mechanics* 123 (1982) 379–398.
- [7] Igarashi, T., Characteristics of the flow around a square prism, *Bulletin of JSME* 27 (1984) 1858–1865.
- [8] A. Sohankar, C. Norberg, L. Davidson, Low Reynolds number flow around a square cylinder at incidence: study of blockage, onset of vortex shedding and outlet boundary condition, *International journal for numerical methods in fluids*, vol. 26, 39±56 (1998).
- [9] D. H. Yoon, K. S. Yang, C. B. Choi, Heat Transfer Enhancement in Channel Flow Using an Inclined Square Cylinder, *Journal of Heat Transfer*, vol 131 (2009).
- [10] M.A. Moussaoui, M. Jami, A. Mezrhab, H. Naji, MRT-Lattice Boltzmann simulation of forced convection in a plane channel with an inclined square cylinder, *International Journal of Thermal Sciences* xxx (2009) 1–12.
- [11] P.M. Coelho, F.T. Pinhoa, A generalized Brinkman number for non-Newtonian duct flows, *J. Non-Newtonian Fluid Mech.* 156 (2009) 202–206.
- [12] Zdravkovich, M.M., *Flow around circular cylinders*, vol. 1: Fundamentals, Oxford University Press, New York (1997).
- [13] Ram Prakash Bharti, R. P. Chhabra, V. Eswaran, A numerical study of the steady forced convection heat transfer from an unconfined circular cylinder, *Heat Mass Transfer* (2007) 43:639–648.